Journal of Hazardous Materials 175 (2010) 680–687

Contents lists available at ScienceDirect

Journal of Hazardous Materials

journal homepage: www.elsevier.com/locate/jhazmat

Reductive dechlorination of γ-hexachlorocyclohexane using Fe–Pd bimetallic nanoparticles

Varima Nagpal [a], Alok D. Bokare [a], Rajeev C. Chikate [b], Chandrashekhar V. Rode [c], Kishore M. Paknikar [a,*]

[a] Center for Nanobioscience, Agharkar Research Institute, G.G. Agarkar Road, Pune 411004, Maharashtra, India
[b] Department of Chemistry, MES Abasaheb Garware College, Karve Road, Pune 411004, India
[c] Chemical Engineering and Process Development Division, National Chemical Laboratory, Pune 411008, India

ARTICLE INFO

Article history:
Received 9 July 2009
Received in revised form
15 September 2009
Accepted 15 October 2009
Available online 6 November 2009

Keywords:
Bimetallic
Nanoparticles
Lindane
Degradation
Kinetics
Cyclohexane

ABSTRACT

Nanoscale Fe–Pd bimetallic particles were synthesized and used for degradation of lindane (γ-hexachlorocyclohexane) in aqueous solution. Batch studies showed that 5 mg/L of lindane was completely dechlorinated within 5 min at a catalyst loading of 0.5 g/L and the degradation process followed first-order kinetics. GC–MS analysis in corroboration with GC-ECD results showed the presence of cyclohexane as the final degradation product. The proposed mechanism for the reductive dechlorination of lindane involves Fe corrosion-induced hydrogen atom transfer from the Pd surface. The enhanced degradation efficiency of Fe–Pd nanoparticles is attributed to: (1) high specific surface area of the nanoscale metal particles (60 m^2/g), manyfold greater that of commercial grade micro- or milli-scale iron particles (~1.6 m^2/g); and, (2) increased catalytic reactivity due to the presence of Pd on the surface. Recycling and column studies showed that these nanoparticles exhibit efficient and sustained catalytic activity.

1. Introduction

Lindane (1,2,3,4,5,6-hexachlorocyclohexane or γ-HCH) is a broad-spectrum pesticide and a persistent pollutant. Its low aqueous solubility, relative high stability, lipophilicity and chlorinated nature contribute to its environmental persistence and resistance to degradation. It is neurotoxic, an endocrine disrupter in humans and is classified by the United States Environment Protection Agency (EPA) and World Health Organization (WHO) as a potent carcinogen and teratogen [1–3]. It has been banned in over 50 countries including Europe and North America. However, India continues to produce and use lindane, with 5387 tonnes technical grade lindane produced from 1995 to 2005. Lindane residues have been detected in drinking water in rural India [4] and human blood samples have shown lindane levels 605 times higher than those found in the United States (average values of 57 and 0.1 ppb for Indian and US samples respectively) [5]. It therefore represents an environmental risk and development of viable methods for its removal from water and food sources are needed.

Conventional methods viz. chemical degradation, physical adsorption, and bioremediation have been reported for the removal of lindane from aqueous solutions. These include use of microwave irradiation and degradation with NaOH-modified sepiolite [6] and addition of hydrogen peroxide [7]. Many researchers have demonstrated the use of microbial cultures for bioremediation of lindane [8–14]. Lindane decomposition *via* sonochemical [15] and gamma ray-induced dechlorination/destruction [16] has also been demonstrated. However, most of these degradation methods lead to the formation of stable but carcinogenic trichlorobenzenes (TCBs) as the major degradation products.

The generation of toxic degradation products and the use of environmentally harsh chemicals lead to several operational constraints, especially for the treatment of lindane-contaminated drinking water. Hence, for effective treatment of pesticide-polluted ground water and surface water, advanced catalytic methods are desirable for complete decomposition of target molecules and elimination of toxic end products. One such method involves use of zero-valent metals for catalytic reductive dehalogenation of various organochlorine compounds like lindane. Among several metals, zero-valent iron is a preferred choice due to its low cost and benign environmental impact [17–19].

Nanoscale iron materials offer a potential advantage over bulk iron due to their large surface areas, which provide more active sites for the reaction, and hence, enhanced reaction rates. But the reduction rate for such highly reactive nano-iron tends to decrease with time due to the formation of oxide layers that block the

* Corresponding author. Fax: +91 20 25651542.
E-mail addresses: paknikar@vsnl.com, kpaknikar@gmail.com (K.M. Paknikar).

0304-3894/$ – see front matter © 2009 Elsevier B.V. All rights reserved.
doi:10.1016/j.jhazmat.2009.10.063

surface-active sites. Incorporation of a second, catalytic metal like Pd, Zn, Ni or Pt onto the iron surface produces enhanced dechlorination rates relative to iron alone [20–24]. Enhanced dehalogenation and prevention of toxic byproduct formation has been observed for iron nanoparticles coated with Pd. Zhang [20] reported 100-fold enhancement in the rate of dechlorination of trichloroethene (TCE) using Pd-coated iron nanoparticles (10–100 nm).

In this work, complete and rapid lindane degradation is reported using palladized iron nanoparticles. Based on GC-ECD and GC–MS analysis, the proposed reductive dechlorination mechanism involves hydrogen atom transfer from the Pd surface to form cyclohexane as the final product. The Fe–Pd nanoparticles showed higher catalytic activity than nano-iron, due to prevention of surface passivation by the presence of Pd. The effects of catalyst loading, repeated exposure of nanoparticles to air/water and continuous flow column study on the lindane degradation efficiency were also examined.

2. Experimental

2.1. Chemicals

The following compounds were used as received: lindane (>99.9%, Sigma, USA), acetone (purity, ~99%, Merck, UK), *n*-hexane (HPLC grade, Qualigens, India), iron (II) sulphate ($FeSO_4{\cdot}7H_2O$, Merck, UK), sodium borohydride ($NaBH_4$, Merck, UK) and palladium acetate ($Pd(COOCH_3)_2$, Aldrich, USA), cyclohexane (Aldrich, USA), sodium carbonate (Na_2CO_3, Aldrich, USA), and sodium bicarbonate ($NaHCO_3$, Aldrich, USA). All reagents and solutions were prepared in ultra-pure water.

2.2. Synthesis of Fe–Pd nanoparticles

Synthesis of iron nanoparticles was achieved by adding 3.1 g of $NaBH_4$ into 6.2 g of $FeSO_4{\cdot}7H_2O$ in 100 mL deionized water according to the procedure of Wang and Zhang [22]. The solution was mixed vigorously under room temperature for 15 min (25 ± 1 °C). Ferrous ion was reduced by borohydride according to the following reaction:

$$2Fe^{2+} + BH_4^- + 2H_2O \rightarrow 2Fe^0 + BO_2^- + 4H^+ + 2H_2 \quad (1)$$

The borohydrate to ferrous ion ratio was 7.4 times of the stoichiometric requirement according to the above equation. Excessive borohydrate was the key factor for rapid and uniform growth of iron nanocrystals [23]. The metal particles formed from the above reaction were washed by repeated cycles (five times) of centrifugation at 5000 r.p.m. and treatment with large volumes (>100 mL/g iron) of ultra-pure water. Palladized Fe particles were prepared by soaking freshly prepared iron nanoparticles in an ethanol solution containing 0.2 wt% of palladium acetate. This caused the reduction and subsequent deposition of Pd on the Fe surface:

$$Fe^0 + Pd^{2+} \rightarrow Fe^{2+} + Pd^0 \quad (2)$$

The palladized iron particles were then vacuum filtered, washed with ethanol and acetone using the centrifugation–washing–centrifugation cycle and finally dried in a vacuum oven at 80 °C.

2.3. Characterization of nanoparticles

Brunnaer–Emmett–Teller (BET) surface area analysis of the synthesized nanoparticles was performed using nitrogen adsorption method with surface analyzer system CHEMBET 3000, Quantichrome Instruments, USA. TEM measurements were performed on a JEOL Model 1200EX instrument operated at an accelerating voltage of 120 kV. Samples for transmission electron microscopic (TEM) were loaded on carbon coated copper TEM grids before being introduced into the vacuum chamber. X-ray diffraction (XRD) analysis of mineralogical characteristics of the nanoparticles was carried out using a Philips diffractometer (Model No. 1730). Nickel filtered Cu-Kα radiation source was used to produce X-ray (λ = 1.542 Å) and scattered radiation was measured with a proportional counter detector at a scan rate of 4°/min. X-ray photoelectron spectroscopy (XPS) analysis was carried out on a VG MicroTech ESCA 3000 instrument using Mg-Kα radiation (photo energy 1253.6 eV) at a pass energy of 50 eV and electron take off angle (angle between electron emission direction and surface plane) of 60°. C 1s spectra was used as a reference with binding energy value of 284.6 eV and the spectra of different samples were corrected for surface charging.

2.4. Batch experiments

All experiments were performed in 30 mL serum bottles with 15 mL of liquid volume. In each batch bottle, 5 mg/L lindane solution was prepared in deionized water (solubility of lindane in water = 8 mg/L). The solution contained a fixed amount of Fe–Pd nanoparticles in the range 0.1–0.5 g/L. The pH of the reaction mixture was ~6.5. All degradation experiments were performed in an open batch system at room temperature (25 ± 2 °C). Solutions were stirred with an agitator to keep the nanoparticle powder suspended. Samples were withdrawn from the bottles at fixed time intervals and extracted into HPLC grade hexane by liquid–liquid extraction process (100 μL of sample was added to 1000 μL hexane, rapidly mixed using ultrasound, and finally the hexane layer was separated). An aliquot of the hexane-extracted sample (0.5 μL) was then analyzed for the degradation of lindane using gas chromatography.

2.5. Lindane degradation and metabolite detection

A gas chromatograph system (ASXL, PerkinElmer, USA) equipped with an electron capture detector (ECD) and a capillary column SGE 3780B21 (length – 25 m, type – bonded phase, material – silica, phase – BP5 non-polar, film thickness – 0.5 μm) was used for degradation studies. The column temperature started at 50 °C, held for 10 min, ramped up to 150 °C at a rate of 10 °C/min, held for 10 min, ramped to 240 °C at a rate of 10 °C/min and finally held for 15 min. The temperature of the injector and detector were maintained at 230 °C and 280 °C respectively. The sample aliquot was eluted with nitrogen carrier gas at 35.0 mL/min. GC–MS analysis was performed on a Trace GC 2000, Thermo Instruments, USA equipped with a Mega 5 MS capillary column (30 m, 0.25 mm ID and 0.5 μm film thickness). The column temperature started at 50 °C, held for 10 min, ramped up to 150 °C at a rate of 10 °C/min, held for 10 min, ramped to 240 °C at a rate of 10 °C/min and finally held for 15 min. Electron impact mass spectrometry was carried out at 70 eV ionization potential and 230 °C ion source temperature. For GC–MS analysis, degradation samples (100 μL) were extracted in HPLC grade toluene (1000 μL) instead of hexane using liquid–liquid extraction to avoid solvent interference during metabolite quantification. Quantification of chloride ions was performed using an ion chromatograph (Dionex DX-120) equipped with a Dionex Ion-Pac column (AS-14) and a conductivity detector. The eluent composition was 3.5 mM Na_2CO_3 + 1 mM $NaHCO_3$.

2.6. Column studies

A small-scale differential column reactor (DCR) was constructed using glass column of 1.5 cm diameter and 30 cm in length for packing of nanoparticles. The column was packed while maintaining the

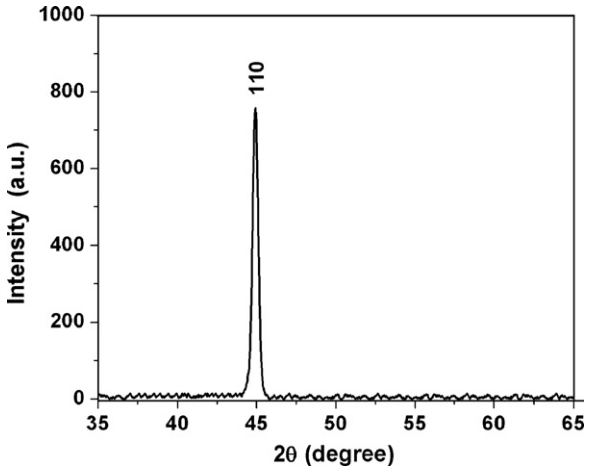

Fig. 1. XRD spectrum of Fe–Pd nanoparticles.

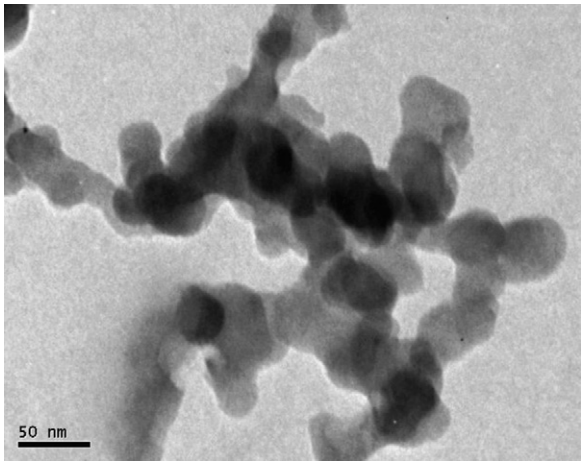

Fig. 2. TEM image of Fe–Pd nanoparticles.

packed materials under ultra-pure water. The differential column containing sand-nanoparticle dual zones was prepared as follows: the column was packed by first filling it with nanopure water and placing a small amount of glass wool at the bottom of the column. Horizontally on top of this glass wool, 5 g of pre-washed beach sand was added. The sand was first sieved through a 2 mm sieve and washed copiously with distilled water till the washings were colorless. The washed sand was then dried at 100 °C overnight. After proper placement of the sand bed, Fe–Pd nanoparticles were added to the column directly as vacuum-dried powder and the total amount added was 10 mg. This value was calculated based on the on the concentration of nanoparticles used in the batch studies (0.5 g/L nanoparticles to degrade 15 mL of lindane aqueous solution). Upon leveling the surface of the nanoparticle bed, another 5 g of sand was placed on top of the nanoparticles. The total amount of sand in the column (10 g) corresponded to a total void volume of 15 mL. Test solution for column experiments containing 5 mg/L lindane was stored in a 2 L glass tank and solutions were pumped through the packed beds using an Ismatec MCP 552 (Switzerland) peristaltic pump. Samples were collected directly from the column effluent tubing into 10 mL glass sample bottles. To match the retention time of lindane in the column with the total time of reaction (5 min), the outflow rate was adjusted to 3 mL/min.

3. Results and discussion

3.1. Nanoparticle characterization

Fig. 1 shows the XRD spectrum of the nanoparticles, showing the presence of bcc Fe^0 at $2\theta = 44.98^o$. However, no peaks corresponding to Pd^0 or Fe-oxide were observed. A mean particle size of 30 nm was calculated using Scherrer equation,

$$t = \frac{0.9\lambda}{B\cos\theta} \quad (3)$$

where t is the median particle size, B is the full width in radians at half-maximum intensity, λ is the X-ray wavelength and θ is the angle at maximum diffraction curve intensity.

The morphology and structure of the Fe–Pd nanoparticles is shown in the TEM images (Fig. 2). The spherical nanoparticles, 25–40 nm in diameter are connected in chains of beads. This observation is due to the magnetic and electronic interactions between the metals [25]. The small size of the nanoparticles can be explained by the low molarity of Fe^{2+}, together with the excess of borohydride used in the synthesizing process. This causes the rapid reduction rate of Fe^{2+} for the formation of more nuclei, and thus less metal atoms are available for particle growth. This produces nano-Fe and subsequently nano-Fe–Pd with small particle size, and high BET surface area (60 m^2/g).

XPS measurements (Fig. 3a and b) showed peaks at 710.6 eV and 724.6 eV, which are characteristic peaks for Fe^{2+} $2p_{3/2}$ and Fe^{2+} $2p_{1/2}$ respectively. A broader peak was observed at 704 eV, which is associated with zero-valent iron (Fe^0 $2p_{3/2}$). The Pd $3d_{5/2}$ core level XPS spectrum showed two peaks at 336.7 and 339.3 eV, which are characteristic peaks of zero-valent palladium (Pd^0). The total iron content in Fe–Pd nanoparticles determined by AAS was 59.2%.

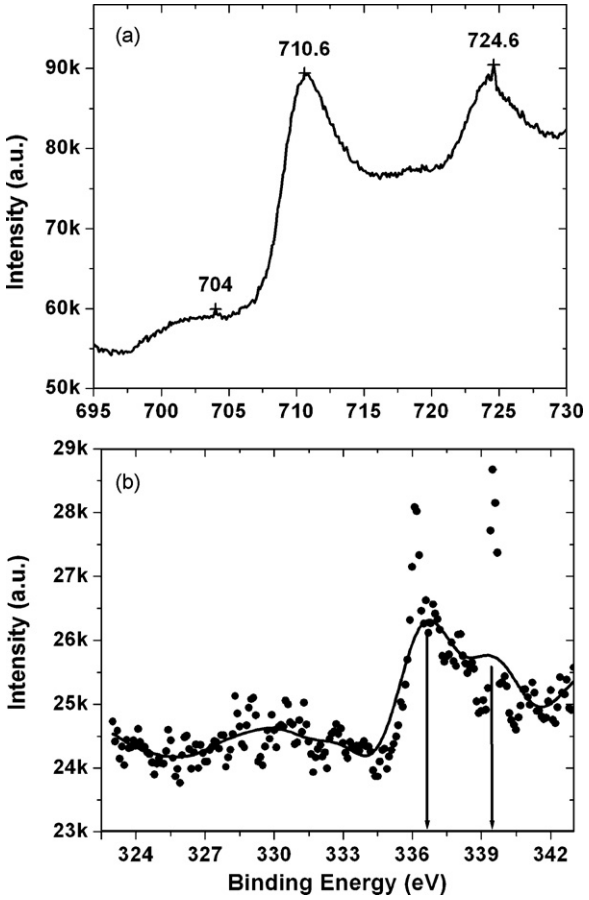

Fig. 3. XPS spectra of (a) Fe 2p core level and (b) Pd $3d_{5/2}$ core level spectra of Fe–Pd nanoparticles. For (b), the black dots and solid black line correspond to the raw data and smoothened data respectively.

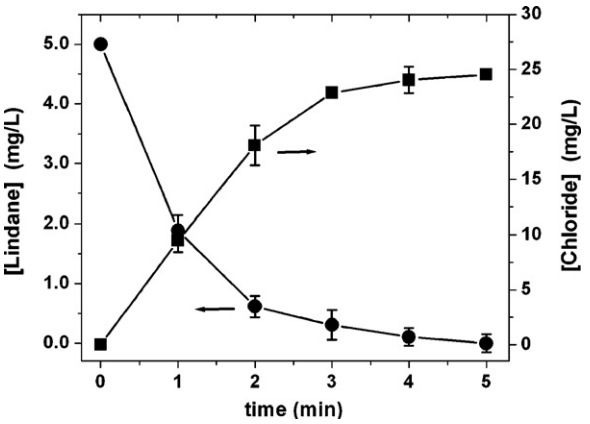

Fig. 4. Kinetics of lindane degradation and chloride generation using Fe–Pd nanoparticles. ([Lindane] = 5 mg/L, [Fe–Pd] = 0.5 g/L, pH 6.5, T = 25 °C).

3.2. Kinetics of lindane degradation

Fig. 4 illustrates the efficiency of these nanoparticles to degrade lindane. A 5 mg/L sample of lindane was completely degraded in 5 min by Fe–Pd (0.5 g/L) within the detection limit of GC-ECD (~10 pg). The degradation of lindane followed a first-order kinetic model:

$$C = C_0 \exp(-k_{obs} t) \quad (4)$$

where C is the lindane concentration at time t, C_0 is the initial lindane concentration, and k_{obs} is the first-order degradation rate constant. Using the above model, the rate constant obtained was $1.02 \pm 0.16\ min^{-1}$. The concomitant increase in chloride ion concentration (Fig. 4) confirmed that lindane was removed from aqueous solution through reductive dechlorination and not *via* adsorption on the nanoparticle surface. However, complete chloride mass balance was not achieved (15% deficit). The chloride ions can be either lost through adsorption or covered by the precipitation of iron hydroxide layers on the nanoparticle surface, as shown previously by Burris et al. [26] and Xu et al. [27]. Alternatively, incomplete chloride mass balance may be also attributed to loss by evaporation of HCl or Cl_2 formed during the degradation process.

To establish the advantage of a palladized nano-iron catalyst, the degradation efficiency of Fe–Pd nanoparticles was compared with iron nanoparticles, commercial bulk iron powder (300 mesh) and palladium-coated bulk iron, under similar experimental conditions. Iron nanoparticles were synthesized using the borohydride reduction process described earlier. Bulk iron powder (0.5 g/L) was pretreated with 6 M HCl for 10 min and washed with ultra-pure water to remove the residual HCl and Fe^{2+}. Palladium-coated bulk iron was prepared by reacting the acid-treated powder with 0.2 wt% palladium acetate. In contrast to the rapid degradation observed by Fe–Pd, the iron nanoparticles exhibited lower degradation efficiency (Fig. 5). Bulk iron powder, on the other hand, did not degrade lindane even at a higher metal concentration (50 g/L) due to the lower surface area (1.6 m^2/g) of the particles. Pd-coated bulk iron showed negligible lindane degradation efficiency.

Although nano-iron provides an increased surface area for the dechlorination reaction compared to bulk iron, the enhanced corrosion rate leads to rapid formation of surface-passivating oxide layers. These oxide layers block the active sites on the catalyst surface and inhibit the dechlorination reaction. Thus, rapid lindane dechlorination occurred at the initial stage (Fig. 5), but the catalytic activity was subsequently inhibited by surface passivation, leading to incomplete degradation. Reductive dechlorination using nano-iron requires direct access of lindane to the iron surface. This can occur only at cracks in the surface oxide/hydroxide film and thus only a small fraction of the iron metal would be available for dechlorination, leading to lower degradation efficiencies. This is consistent with the findings of Farrell et al. [28], who showed that trichloroethylene dechlorination rates on cathodically protected iron were 2–3 orders of magnitude faster than those on oxide-coated iron. On iron coated with electrically conductive magnetite or semiconducting Fe(III) oxides, halocarbon reduction may also occur *via* electron tunneling through the oxides [29,30]. In the present study, however, rapid oxide layer formation and the absence of any deliberately coated electrically conducting oxide film on the surface inhibited direct electron transfer from the iron surface to lindane.

In the Fe–Pd bimetallic system, the rapid oxidation of iron to generate electrons and hydrogen is similar to the corrosion process in nano-Fe. However, the surface Pd catalyzes the adsorption and dissociation of hydrogen to form surface Pd-hydrides, which are powerful reducing agents [31]. It is also known that iron oxidizes faster when it is in contact with a less active (noble) metal like Pd [32]. Thus, iron is preferably oxidized (acts as anode) whereas palladium is protected (acts as cathode). The subsequent formation of galvanic cells between the coupled iron and palladium species results in continuous electron flow and enhanced catalytic activity. The importance of active surface sites (like Pd), capable of utilizing hydrogen in the dechlorination reaction, has been demonstrated by Liu et al. for TCE dechlorination [33]. Since Pd reduces surface passivation by oxide layers and promotes adsorption–dissociation of hydrogen gas into strongly reducing atomic hydrogen, Fe–Pd offers a double advantage over nano-iron.

3.3. Product identification and degradation mechanism

GC–MS analysis of the lindane solution treated with Fe–Pd nanoparticles showed the presence of cyclohexane as the final degradation product. No additional chlorinated intermediates or products were detected, which corroborated with the GC-ECD results. The kinetics of lindane degradation and cyclohexane formation are shown in Fig. 6. The simultaneous generation of cyclohexane and chloride ions (Fig. 4) indicated that lindane degradation with Fe–Pd followed a sequential reduction process through the replacement of all chlorines atoms by hydrogen (hydrodechlorination).

Dechlorination reactions on Fe–Pd catalyst occur by adsorption of the chlorinated compound (like lindane) on the particle surface [31]. The Pd on the surface acts as a collector of hydrogen gas produced *via* reduction of water by iron, i.e., the iron corrosion

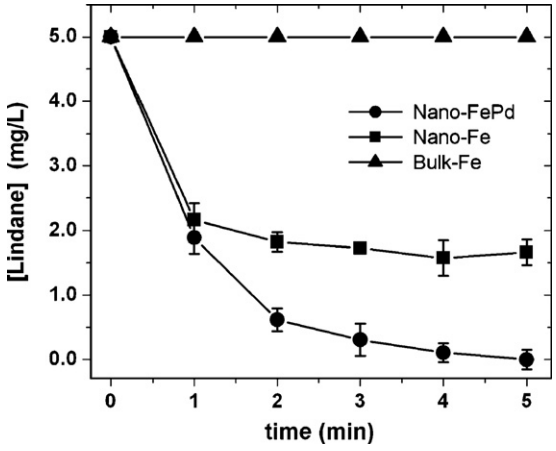

Fig. 5. Comparison of lindane degradation using Fe–Pd nanoparticles, iron nanoparticles and commercial bulk iron. ([Lindane] = 5 mg/L, [catalyst] = 0.5 g/L, pH 6.5, T = 25 °C).

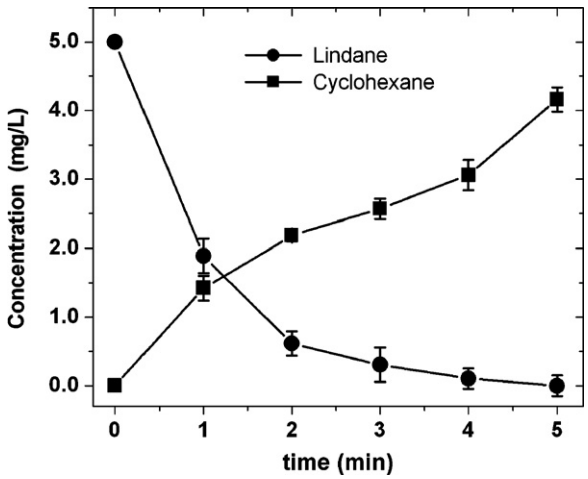

Fig. 6. Kinetics of lindane degradation and cyclohexane formation using Fe–Pd nanoparticles. ([Lindane] = 5 mg/L, [Fe–Pd] = 0.5 g/L, pH 6.5, T = 25 °C).

reaction:

$$Fe^0 + 2H_2O \rightarrow Fe^{2+} + H_2 + 2OH^- \quad (5)$$

On the Pd surface, the diatomic dissociation of H_2 can lead to the formation of metal hydride for the dechlorination reaction:

$$2Pd^0 + H_2 \rightarrow 2Pd\text{–}H \quad (6)$$

The C–Cl bond of the adsorbed lindane is then broken, and hydrogen provided by the active metal hydride replaces all the chlorine atoms to form cyclohexane:

$$6Pd\text{–}H + C_6H_6Cl_6 \rightarrow 6Pd^0 + C_6H_{12} + 6Cl^- \quad (7)$$

Alternatively, dissociation of H_2 gas on Pd can lead to formation of hydrogen radicals:

$$Pd^0 + H_2 \rightarrow 2H^\bullet \quad (8)$$

These hydrogen radicals are highly reactive to C–Cl bonds and thus, radical-induced lindane dechlorination to form cyclohexane is also possible.

In our knowledge, this is the first report of cyclohexane formation during lindane dechlorination using heterogeneous metallic and bimetallic catalysts. Prior studies have shown that lindane was dechlorinated to benzene and chlorobenzene by Fe–Cu, Al–Cu and Mg–Cu [34]. Also, lindane dechlorination using Pd nanoparticles [35] and Pd-doped Al_2O_3 [36] generated benzene as the final degradation product. Wang et al. [37] also reported that lindane dechlorination using granular zero-valent iron led to the formation of benzene (major) and chlorobenzene (minor) as the main products. In the case of zero-valent iron, direct electron transfer from the metal surface results in sequential elimination of two chlorine atoms (dichloroelimination) or one HCl molecule (dehydrochlorination) to form chlorobenzene and/or benzene [38]. Moreover, the formation of benzene in the bimetallic systems also suggests that the role of second metal was limited to prevention of surface passivation and sustained electron flow. In the present study also, GC–MS analysis of the lindane solution treated with nano-Fe confirmed the presence of benzene as the sole degradation product (data not shown).

However, in the Fe–Pd bimetallic system, the dechlorination process is initiated by the Pd-mediated dissociation of H_2 into H atoms, which replace the chlorine atoms on the lindane molecule (hydrodechlorination). The importance of Pd as the hydrogen-activation catalyst is evident from the fact that lindane degradation by bimetallic Fe–Cu generated benzene and not cyclohexane as the final product [34]. The high hydrogen adsorption–dissociation capacity of Pd (900 times its own volume) and the formation of cyclohexane imply that the deposited metal on the iron surface critically governs the lindane dechlorination pathway in Fe-based bimetallic systems. Interestingly though, both Pd^0 nanoparticles [35] and Pd^0-on-Al_2O_3 [36] in the presence of externally added H_2 gas generated benzene and not cyclohexane during lindane dechlorination. Although lindane dechlorination by heterogeneous Pd-based catalysts involves hydrogenation *via* H_2 activation, the formation of cyclohexane using Fe–Pd nanoparticles and benzene using Pd^0 and Pd/Al_2O_3 indicates the crucial role of (a) catalyst type/nature of support, (b) source of H_2, (c) the presence/absence of bimetallic structure, and/or (d) acido-basic properties of the catalyst, in deciding the mechanistic pathway.

The selectivity in product formation by Pd-mediated hydrogenation (selective hydrogenation) is strongly influenced by the catalyst properties such as Pd particle morphology, crystallographic orientations of Pd on the support surface and its electronic character [39]. Also, the electronic and geometric structure of Pd is ultimately dependent on the choice of the support (oxides like Al_2O_3, SiO_2 or activated carbon or graphite) [40], which subsequently influences the nature of the chemisorbed intermediate(s) [41] and product selectivity. The bimetallic nature of Fe–Pd nanoparticles would also affect the electronic properties of Pd, due to the formation of a galvanic cell between the two metals. The different electronic interactions in Fe–Pd and Pd^0/Al_2O_3 catalysts may contribute to dissimilar lindane adsorption orientations and reactivity, leading to different products (cyclohexane or benzene). Additionally, the nature of the final product is also affected by the nature of the active hydrogen species (hydrogen emerging from the bulk of the Pd metal or surface hydrogen [42]).

In case of Fe–Pd nanoparticles, the bimetallic contact between the two metals on the iron surface and the evolution of H_2 on the iron particles (Eq. (5)) may generate active hydrogen species in the Pd bulk. In contrast, the Pd^0 and Pd^0/Al_2O_3 systems utilize externally added H_2, wherein formation of surface-active hydrogen species is more probable. Since surface hydrogen is less energetic compared to those generated in bulk Pd, it provides better product selectivity in hydrogenation reactions [43]. Finally, the acid–base properties of the catalyst support (especially oxides like Al_2O_3 and corrosive metals like Fe) are strongly affected by the solution pH, which changes the adsorption–desorption equilibrium of the surface-adsorbed species (reactant, intermediates and product) [44]. Thus, all these factors, alone or in combination, may contribute to different lindane dechlorination pathways and final product profiles for Fe–Pd bimetallic nanoparticles and Pd^0 or Pd^0/Al_2O_3.

3.4. Effect of Fe–Pd mass concentration

Since the dechlorination reaction is a surface-mediated process, the nanoparticle surface area can affect the dechlorination rate. As the Fe–Pd mass concentration is increased, the concentration of reactive Fe and Pd sites will increase simultaneously. This should lead to increased total surface area and enhanced dechlorination activity. Fig. 7 shows the effect of Fe–Pd mass concentration on the lindane degradation efficiency. Although the degradation rate constant (k_{obs}) increased linearly with Fe–Pd concentration, the relationship between k_{obs} and [Fe–Pd] is not first order. For instance, at Fe–Pd concentration of 0.1 g/L, the k_{obs} value is 0.65 min^{-1}. A first-order relationship would require that a two-fold increase in Fe–Pd loading leads to a two-fold increase in the k_{obs} value. However, a k_{obs} value of 0.7 min^{-1} is obtained at 0.2 g/L nanoparticles concentration. In the case of iron-based catalysts, the relationship between the rate constant and catalyst concentration can be first order only if (a) fraction of redox-active

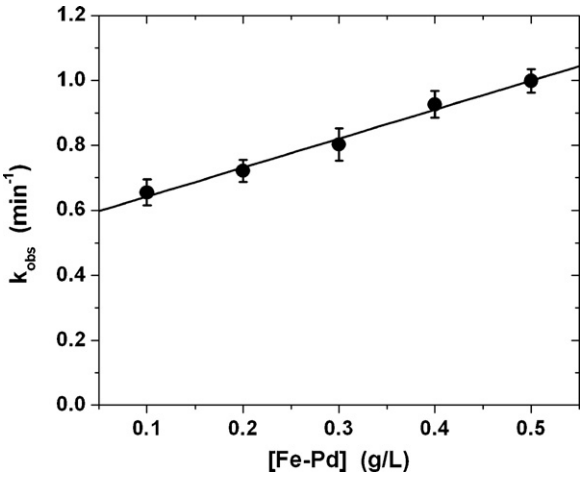

Fig. 7. Effect of Fe–Pd concentration on lindane degradation. [Lindane] = 5 mg/L, pH 6.5, T = 25 °C.

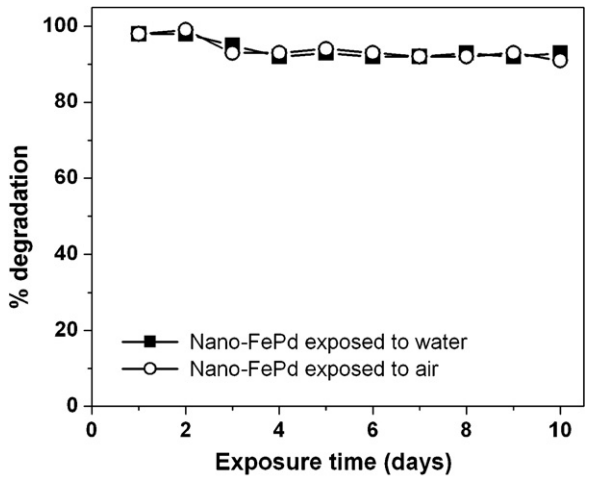

Fig. 8. Lindane degradation efficiency of recycled Fe–Pd nanoparticles exposed to air. ([Lindane] = 5 mg/L, [Fe–Pd] = 0.5 g/L, pH 6.5, T = 25 °C).

total iron surface area, and (b) the intrinsic reactivity of iron, is essentially constant for all catalyst concentrations. Cwiertny and Roberts [45] have reported that the fraction of active iron surface area remains constant with change in iron particle loading, even under mass-transfer-limiting conditions. However, the intrinsic reactivity of iron is critically dependent on the corrosion rate, changes in solution pH, and rate and/or extent of surface passivation. With increasing Fe–Pd concentration, the total surface area available for iron corrosion increases, leading to increase in solution pH. This subsequently leads to enhance surface passivation and thus, the intrinsic reactivity of iron cannot remain constant at all catalyst concentrations. This results in a non-linear behavior between the lindane degradation rate constant and Fe–Pd concentration.

3.5. Efficiency of the recycled catalyst

In order to test the economy of the reductive degradation process, which is a measure of the number of times the catalyst can be reused without sacrificing its efficiency, the life span of the Fe–Pd nanoparticles was tested. Repeated use of nanoparticles after continuous exposure to air and water was studied to correlate the reaction rate with the status of the catalyst surface and its reactivity. After the first degradation cycle, the treated solution was kept standing for 24 h and then the aqueous supernatant was decanted. The particles were then washed thoroughly with distilled water and reused for degradation of a fresh lindane sample. In parallel, immediately after the first cycle, the lindane solution was decanted. The nanoparticles were exposed to air for 24 h and then reused for degradation of a fresh lindane sample. The results for a 5-min degradation reaction using the air-exposed nanoparticles are shown in Fig. 8. A similar profile was obtained for the Fe–Pd nanoparticles exposed to water. The reactivity of the nanoparticles decreased slightly over a period of 10 days, with the lindane degradation efficiency dropping to ~92% after 10 days. However, this data is for a 5-min reaction time only and, hence, a ~6–8% decrease in the degradation activity can be compensated by increasing the reaction time. In an additional experiment, the 10-day-old catalyst was reacted with a fresh lindane sample with an increase in reaction time to 10 min. The catalyst showed 100% lindane degradation efficiency. These results show that Fe–Pd nanoparticles showed good reactivity even after continuous exposure to air and water. However, repeated lindane degradation cycles for longer exposure time (more than 3–4 months) and simultaneous SEM/TEM imaging of the surface-exposed particles need to be performed to establish the long-term stability and shelf life of these nanoparticles.

3.6. Continuous flow column studies

The high catalytic efficiency and excellent stability of Fe–Pd nanoparticles for lindane degradation was established for lab-scale volumes only. But, performance of these nanoparticles for large-scale applications depends on efficient treatment of large volumes of contaminated aqueous solutions. was treated with Fe–Pd nanoparticles in a continuous flow column mode. Continuous flow column experiments using a fixed-particle, dual-zone bed (beach sand + nanoparticles) were undertaken to provide a quantitative estimate of the absolute volume of lindane aqueous solution, which can be treated efficiently using a single batch of Fe–Pd nanoparticles.

The capacity of Fe–Pd nanoparticles for lindane degradation under dynamic flow conditions was determined using a breakthrough curve (Fig. 9). The gradual loss in activity of Fe–Pd nanoparticles can be explained in terms of iron corrosion-induced increase in pH, which leads to passivation of the catalyst surface Since, all lindane degradation experiments were carried out at near-neutral pH, continuous iron corrosion leads to generation of hydroxyl ions (Eq. (5)) and increases the pH. This causes the precip-

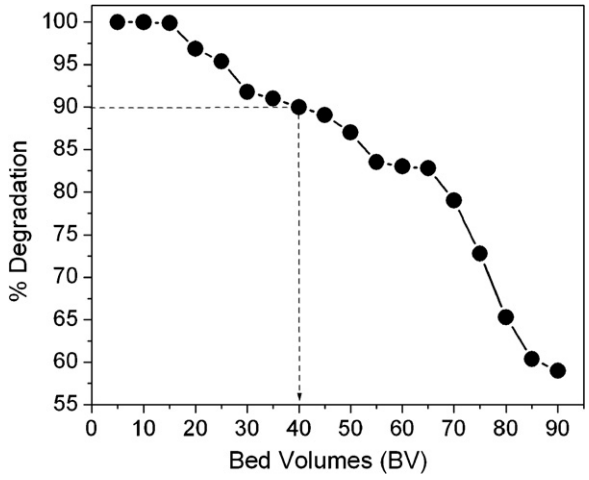

Fig. 9. Breakthrough curve for lindane in a Fe–Pd nanoparticles fixed-bed column.

itation of Fe^{2+} ions on the surface as Fe^{2+}-hydroxides/oxides, which can prevent or reduce contact between surface palladium and lindane, or cause palladium to lose contact with the base iron metal. Under these circumstances, generation of Pd-hydride and lindane hydrodechlorination is inhibited and catalytic efficiency gradually decreases.

The breakthrough point (BP) is defined as the time when the effluent concentration (C) reaches a percentage of the influent concentration (C_0), which is considered unacceptable, e.g., 10% (90% degradation or $C/C_0 = 0.1$) [46]. For $C/C_0 = 0.1$, the total number of bed volumes (BV) passed through the nanoparticles zone were 40. No adsorption or degradation of lindane on the sand bed alone was observed. The total number of BV treated at BP is a measure of the total lindane concentration degraded using a fixed-bed nanoparticles zone under continuous flow. Thus, at a flow rate of 3 mL/min and a single bed volume containing 5 mg/L lindane, the total mass of lindane degraded in aqueous solution using 0.5 g/L Fe–Pd nanoparticles at breakthrough point was 200 mg. The total iron concentration in the column effluent measured by AAS after 90 bed volumes was 81 μg/L (or 81 ppb). Thus, the total iron leached out in the column effluent was 0.004% of the total concentration in the nanoparticles (1850 mg/L for 10 mg nanoparticles). The palladium concentration in the effluent was not detectable due to the inherent low concentration in the nanoparticles (0.2 wt%). The very low iron concentration in the column effluent indicates that all nanoparticles and majority of the iron species generated through corrosion were retained inside the packed sand bed.

In summary, rapid and complete dechlorination of lindane in aqueous solution was achieved using Fe–Pd bimetallic nanoparticles. The degradation reaction followed first-order kinetics, but the dechlorination rate constant showed non-first-order dependence on the nanoparticles concentration. GC–MS analysis showed the presence of cyclohexane as the final product, which indicated that surface Pd-mediated lindane hydrodechlorination was the prevalent degradation pathway. The potential advantages of Fe–Pd nanoparticles for treatment of lindane aqueous solutions include: (1) High surface area, (2) Enhanced catalytic activity, (3) First demonstration case in which lindane dechlorination does not yield toxic intermediates such as 1,2,4-trichlorobenzene and/or chlorinated benzenes at ambient reaction conditions, and (5) long efficient life span.

Although, the gradual loss of Fe^0 and oxide layer formation in Fe–Pd nanoparticles are severe drawbacks, the *in situ* generation of H_2 for hydrogenation provides a huge advantage for *in situ* pollutant degradation. In contrast, both Pd^0 and Pd/Al_2O_3 require external H_2 addition with high concentrations and pressures. This offsets the advantage offered by continuous reactivity and enhanced catalyst stability. Also, continuous hydrogen bubbling for Pd/Al_2O_3 systems during on-site applications is costly and requires additional infrastructural facilities. This also decreases the overall cost-benefit achieved by sustained catalyst activity, long-term stability and reusability. In case of Fe–Pd nanoparticles, the abundance and cheap cost of iron may allow use of multiple catalyst batches during a single treatment cycle to compensate for activity loss. Thus, Fe–Pd nanoparticles offer potential advantages for *in situ* applications (as permeable reactive barriers for groundwater treatment or as injectable catalysts for soil remediation), while [$Pd/Al_2O_3 + H_2$] systems are superior catalysts for *ex situ* applications (treatment of industrial effluents and wastewater)".

Acknowledgements

V. Nagpal thanks the Council of Scientific and Industrial Research, Government of India, for the award of Senior Research Fellowship. A.D. Bokare and K.M. Paknikar acknowledge Nano Cutting Edge Technology Pvt. Ltd. for financial support and Agharkar Research Institute for providing infrastructural support.

References

[1] R.C.W. Hall, R.C.W. Hall, Long term psychological and neurological complications of lindane poisoning, Psychosomatics 40 (1999) 513–517.
[2] L. Silvestroni, S. Palleschi, Effects of organochlorine xenobiotics on human spermatozoa, Chemosphere 39 (1999) 1249–1252.
[3] World Health Organization, Environment Health Criteria 124: Lindane, International Programme on Chemical Safety, WHO EHC, 1991.
[4] International HCH and Pesticides Association, The Legacy of Lindane HCH Isomer Production. A Global Overview of Residue Management, Formulation and Disposal, 2006.
[5] http://www.cseindia.org/aboutus/press_releases/press_20050607.htm.
[6] R. Salvador, B. Casal, M. Yates, M.A. Martín-Luengo, E. Ruiz-Hitzky, Microwave decomposition of a chlorinated pesticide (lindane) supported on modified sepiolite, Appl. Clay Sci. 22 (2002) 103–113.
[7] U. Ahlborg, T.M. Thunberg, Chlorinated phenols: occurrence, toxicity, metabolism and environmental impact, CRC Crit. Rev. Toxicol. 7 (1980) 1–35.
[8] S.K. Sahu, K.K. Patnaik, M. Sharmila, N. Sethunathan, Degradation of alpha-, beta- and gamma-hexachlorocyclohexane by a soil bacterium under aerobic conditions, Appl. Environ. Microbiol. 56 (1990) 3620–3622.
[9] A.W. Boyle, M.M. Haggblom, L.Y. Young, Dehalogenation of lindane (γ-hexachlorocyclohexane) by anaerobic bacteria from marine sediments and by sulphate-reducing bacteria, FEMS Microbiol. Ecol. 29 (1999) 379–387.
[10] T.M. Phillips, A.G. Seech, H. Lee, J.T. Trevors, Colorimetric assay for lindane dechlorination by bacteria, J. Microbiol. Methods 47 (2001) 181–188.
[11] T.K. Adhya, S.K. Apte, K. Raghu, N. Sethunathan, N.B.K. Murthy, Novel polypeptides induced by the insecticide lindane (γ-hexachlorocyclohexane) are required for its biodegradation by a sphingomonas paucimobilis strain, Appl. Environ. Microbiol. 221 (1996) 755–761.
[12] S.F. Pesce, D.A. Wunderlin, Biodegradation of lindane by a native bacterial consortium isolated from contaminated river sediment, Int. Biodeter. Biodegr. 54 (2004) 255–260.
[13] W.W. Mohn, B. Mertens, J.D. Neufeld, W. Verstraete, V. de Lorenzo, Distribution and phylogeny of hexachlorocyclohexane-degrading bacteria in soils in Spain, Environ. Microbiol. 8 (2006) 60–68.
[14] B. Mertens, N. Boon, W. Verstraete, Stereospecific effect of hexachlorocyclohexane on activity and structure of soil methanotrophic communities, Environ. Microbiol. 7 (2005) 660–669.
[15] W.J. Catallo, T. Junk, Sonochemical dechlorination of hazardous wastes in aqueous system, Waste Manage. 15 (1995) 303–309.
[16] B.J. Mincher, D.H. Meikrantz, R.J. Murphy, G.L. Gresham, M.J. Connolly, Gamma ray induced degradation of polychlorobiphenyls and pesticides using spent reactor fuel, Int. J. Rad. Appl. Instr. A 42 (1991) 1061–1065.
[17] Y. Kim, E.R. Carraway, Dechlorination of pentachlorophenol by zero valent iron and modified zero valent irons, Environ. Sci. Technol. 34 (2000) 2014–2017.
[18] D.W. Blowes, C.J. Ptacek, S.G. Benner, C.W.T. McRae, R.W. Puls, Treatment of inorganic contaminants using permeable reactive barriers, J. Contam. Hydrol. 45 (2000) 123–127.
[19] J. Farrell, W.D. Bostick, R.J. Jarabek, J.N. Fiedor, Uranium removal from ground water using zero valent media, Ground Water 37 (1999) 618–624.
[20] W.-X. Zhang, Nanoscale iron particles for environmental remediation: an overview, J. Nanoparticle Res. 5 (2003) 323–332.
[21] B. Schrick, B.W. Hydutsky, J.L. Blough, T.E. Mallouk, Delivery vehicles for zero valent metal nanoparticles in soil and groundwater, Chem. Mater. 16 (2004) 2187–2193.
[22] C.-B. Wang, W.-X. Zhang, Synthesizing nanoscale iron nanoparticles for rapid and complete dechlorination of TCEs and PCBs, Environ. Sci. Technol. 31 (1997) 2154–2156.
[23] L. Liang, N.E. Korte, G.D. Goodlaxson, J. Clausen, Q. Fernando, R. Muftikian, Byproduct formation during the reduction of TCE by zero-valence iron and palladized iron, Ground Water Monit. Rem. 17 (1997) 122–127.
[24] W.-X. Zhang, C.-B. Wang, H.-L. Lien, Treatment of chlorinated organic contaminants with nanoscale bimetallic nanoparticles, Catal. Today 40 (1998) 387–395.
[25] L. Zhang, A. Manthiram, Chains composed of nanosize metal particles and identifying the factors driving their formation, Appl. Phys. Lett. 70 (1997) 2469–2473.
[26] D.R. Burris, T.J. Campbell, V.S. Manoranjan, Sorption of trichloroethylene and tetrachloroethylene in a batch reactive metallic iron–water system, Environ. Sci. Technol. 29 (1995) 2850–2855.
[27] X. Xu, H. Zhou, P. He, D. Wang, Catalytic dechlorination kinetics of p-dichlorobenzene over Pd/Fe catalysts, Chemosphere 58 (2005) 1135–1140.
[28] J. Farrell, W.D. Bostick, R.J. Jarabek, J.N. Fiedor, Investigation of the long-term performance of zero-valent iron for reductive dechlorination of trichloroethylene, Environ. Sci. Technol. 37 (2000) 618–620.
[29] B. Balco, P.G. Tratnyek, Photoeffects on the reduction of carbon tetrachloride by zero-valent iron, J. Phys. Chem. B 102 (1998) 1459–1465.
[30] M.M. Scherer, B.B. Balco, P.G. Tratnyek, The role of oxides in reduction reactions at the metal-water interface, in: Mineral-Water Interfacial Reactions: Kinetics and Mechanisms, ACS Symposium Series 715, American Chemical Society, Washington, DC, USA, 1998, pp. 301–332.

[31] Y.-H. Tee, L. Bachas, D. Bhattacharya, Degradation of trichloroethylene and dichlorobiphenyls by iron-based bimetallic nanoparticles, J. Phys. Chem. C 113 (2009) 9454–9464.
[32] M.G. Fontana, R.W. Staehle, Advances in Corrosion Science and Technology, Plenum, New York, 1980.
[33] Y. Liu, S.A. Majetich, R.D. Tilton, D.S. Sholl, G.V. Lowry, TCE dechlorination rates, pathways, and efficiency of nanoscale iron particles with different properties, Environ. Sci. Technol. 39 (2005) 1338–1345.
[34] C. Schlimm, E. Heitz, Development of a wastewater treatment process: reductive dehalogenation of chlorinated hydrocarbons by metals, Environ. Prog. 15 (1996) 38–47.
[35] B. Mertens, C. Blothe, K. Windey, W.D. Windt, W. Verstraete, Biocatalytic dechlorination of lindane by nano-scale particles of Pd(0) deposited on *Shewanella oneidensis*, Chemosphere 66 (2007) 99–105.
[36] C. Schüth, M. Reinhard, Hydrodechlorination and hydrogenation of aromatic compounds over palladium on alumina in hydrogen-saturated water, Appl. Catal. B 18 (1998) 215–221.
[37] Z. Wang, P. Peng, W. Huang, Dechlorination of γ-hexachlorocyclohexane by zero-valent metallic iron, J. Hazard. Mater. 166 (2009) 992–997.
[38] X. Liu, P. Peng, J. Fu, W. Huang, Effects of FeS on the transformation kinetics of γ-hexachlorocyclohexane, Environ. Sci. Technol. 37 (2003) 1822–1828.
[39] C. Park, M.A. Keane, Catalyst support effects: gas-phase hydrogenation of phenol over palladium, J. Colloid Interface Sci. 266 (2003) 183–194.
[40] M.-M. Yu, M. Sheintuch, Catalytic fibers and cloths, Appl. Catal. A 231 (2002) 1–16.
[41] I. Efremenko, Implication of palladium geometric and electronic structures to hydrogen activation on bulk surface and clusters, J. Mol. Catal. A 173 (2001) 19–59.
[42] D. Teschner, E. Vass, M. Hävecker, S. Zafeiratos, P. Scnörch, H. Sauer, A. Knop-Gericke, R. Schlögl, M. Chamam, A. Wootsch, A.S. Canning, J.J. Gamman, S.D. Jackson, J. McGregor, L.F. Gladden, J. Catal. 242 (2006) 26–37.
[43] A.M. Doyle, S.K. Shaikhutdinov, S.D. Jackson, H.J. Freund, Hydrogenation on metal surfaces: why are nanoparticles more active than single crystals? Angew. Chem. Int. Ed. 42 (2003) 5240–5243.
[44] S. Scirè, S. Minicò, C. Crisafulli, Selective hydrogenation of phenol to cyclohexanone over supported Pd and Pd–Ca catalysts: an investigation on the influence of different supports and Pd precursors, Appl. Catal. A 235 (2002) 21–31.
[45] D.M. Cwiertny, A.L. Roberts, On the non-linear relationship between k_{obs} and reductant mass loading in iron batch systems, Environ. Sci. Technol. 39 (2005) 8948–8957.
[46] V.J. Inglezakis, M.D. Loizidou, H.P. Grigoropoulou, Equilibrium and kinetic ion exchange studies of Pb2+, Cr3+, Fe3+, and Cu2+ on natural clinoptilolite, Water Res. 36 (2002) 2784–2792.